Applied Catalysis B: Environmental 312 (2022) 121442

Contents lists available at ScienceDirect

Applied Catalysis B: Environmental

journal homepage: www.elsevier.com/locate/apcatb

Heterogeneous photo-electro-Fenton degradation of tetracycline through nitrogen/oxygen self-doped porous biochar supported $CuFeO_2$ multifunctional cathode catalyst under visible light

Shuaishuai Xin [a,b,c], Siyue Huo [a,c], Yanjun Xin [b], Mengchun Gao [a,c,*], Yanhao Wang [a,c], Wenjie Liu [a], Chunlei Zhang [a,c], Xiaoming Ma [a,c]

[a] Key Lab of Marine Environment and Ecology, Ministry of Education, Ocean University of China, Qingdao 266100, China
[b] Qingdao Engineering Research Center for Rural Environment, College of Resources and Environment, Qingdao Agricultural University, Qingdao 266109, China
[c] Shandong Provincial Key Laboratory of Marine Environment and Geological Engineering, Ocean University of China, Qingdao 266100, China

ARTICLE INFO

Keywords:
Heterogeneous photo-electro-Fenton
Nitrogen/oxygen self-doped porous biochar
$CuFeO_2$
Tetracycline
Toxicity estimation

ABSTRACT

The nitrogen/oxygen self-doped porous biochar (NO/PBC) and NO/PBC supported $CuFeO_2$ ($CuFeO_2$-NO/PBC) were prepared and mixed as cathode catalysts for gas diffusion electrode (GDE) fabrication. The fabricated GDE could realize H_2O_2 electrogeneration and activate H_2O_2 to produce active radicals through NO/PBC and $CuFeO_2$, respectively. The GDE with the NO/PBC to $CuFeO_2$-NO/PBC ratio of 1:1 ($CuFeO_2$-NO/PBC-GDE-1.0) possessed more superior catalytic performance for tetracycline degradation in heterogeneous photo-electro-Fenton (hetero-PEF) system under visible light than other as-fabricated GDEs. The $^{\bullet}OH$ was primary species, and $^{\bullet}O_2^-$ was auxiliary species for hetero-PEF degradation of tetracycline through $CuFeO_2$-NO/PBC-GDE-1.0. The electron on the cathode surface and photoinduced electron could accelerate $\equiv Fe^{3+}/\equiv Fe^{2+}$ and $\equiv Cu^{2+}/\equiv Cu^{+}$ redox cycle, promoting $^{\bullet}OH/^{\bullet}O_2^-$ production and tetracycline degradation. The toxicity estimation of tetracycline and intermediates, TOC removal and *Escherichia coli* growth inhibition confirmed that the remission of overall toxicity, the inhibition of antibacterial property and the mineralization of tetracycline were achieved in hetero-PEF system.

1. Introduction

Antibiotics have been widely applied in clinical or/and non-clinical treatments [1]. Tetracycline, as a kind of broad-spectrum antibiotics, is frequently detected in aquatic environment due to the indiscriminate discharge of pharmaceutical wastewater. The overuse of tetracycline leads to the occurrence of drug-resistant bacteria, which may affect human health and ecosystem [2]. Numerous techniques have been developed to remove tetracycline in the water, including adsorption [3], membrane filtration [4], biodegradation [5] and advanced oxidation processes (AOPs) [6–10]. The adsorption and membrane filtration can only achieve the phase transfer of tetracycline, and cannot realize harmless treatment. The biodegradation efficiency of tetracycline is very slow due to its complex structure and bio-resistant property. Comparatively, AOPs possess favorable ability for producing highly effective reactive oxygen species, have been considered the most attractive strategies for tetracycline degradation.

Electrochemical AOPs based on unselective degradation of organic pollutants by highly active $^{\bullet}OH$ ($(E_0(^{\bullet}OH/H_2O) = +2.8\ V_{NHE}$), have deserved increasing attention in organic wastewaters remediation owing to high mineralization performance, convenient operation and minimal chemical additives [11,12]. Especially, electro-Fenton (EF) has been suggested impressive ability for organic pollutants degradation since the in-situ electrogeneration of H_2O_2 can be achieved through 2-electron oxygen reduction reaction (ORR) on a suitable cathode (Eq. 1), and further react with added iron ions (Eqs. 2–4) to produce oxidative radicals (i.e., $^{\bullet}OH$, $^{\bullet}O_2H$ and $\bullet O_2^-$) [13,14].

$$O_2 + 2H^+ + 2e^- \rightarrow H_2O_2 \quad (1)$$

$$Fe^{2+} + H_2O_2 + H^+ \rightarrow Fe^{3+} + \bullet OH + H_2O \quad (2)$$

$$Fe^{3+} + H_2O_2 \rightarrow Fe^{2+} + \bullet O_2H \quad (3)$$

* Corresponding author at: Key Lab of Marine Environment and Ecology, Ministry of Education, Ocean University of China, Qingdao 266100, China.
E-mail address: mengchungao@outlook.com (M. Gao).

https://doi.org/10.1016/j.apcatb.2022.121442
Received 23 February 2022; Received in revised form 4 April 2022; Accepted 21 April 2022
Available online 25 April 2022

$$\bullet O_2H \leftrightarrow \bullet O_2^- + H^+ \quad (4)$$

The in-situ electrogeneration of H_2O_2 can avoid potential risks and expensive costs related to the transportation, storage and operation of concentrated H_2O_2 [15]. It is well acknowledged that cathode catalyst acts a key role in H_2O_2 electrogeneration and EF efficiency. In recent decades, carbon materials are regarded as effective metal-free cathode catalyst for H_2O_2 generation due to lower costs, rich reserves and fine electrochemical stability, such as carbon black [16], acetylene black [17], activated carbon [18], graphite [19] and biochar [20]. Among them, biochar can be prepared from renewable and sustainable biomass source, which has recently attracted increasing attention in the field of H_2O_2 generation due to the existence of heteroatoms (especially nitrogen and oxygen elements) [20–22]. Previous researches have confirmed that the oxygen and/or nitrogen functional groups in carbon-based catalyst could evidently improve the performance of H_2O_2 electrogeneration [23–25]. Alfalfa with high content of protein is regarded as a suitable raw material for the preparation of nitrogen and/or oxygen self-doped multifunctional biochar [26–28]. Our previous research has verified that the prepared nitrogen/oxygen self-doped porous biochar (NO/PBC) by alfalfa as raw material showed satisfactory 2-electron ORR selectivity for H_2O_2 generation [29]. Therefore, the NO/PBC was chosen as cathode catalyst for H_2O_2 electrogeneration by 2-electron ORR pathway in the present work.

Traditional homogeneous EF process is still confronted with great challenge due to harsh reaction conditions, loss of soluble iron ions and production of iron sludges. To overcome these intrinsic drawbacks, various researches are performed to develop solid iron-based catalysts in heterogeneous EF-like (hetero-EF) process for replacing the soluble iron ions, such as goethite [30], pyrite [31], hematite [32] and zero-valent iron nanoparticles [33]. This strategy can broaden the pH application range of traditional EF technique and realize clean reaction process using recovered solid catalysts [8]. However, the degradation efficiency of organic pollutant by monometallic iron-based catalysts in hetero-EF process is unsatisfactory due to low regeneration efficiency of Fe(II) on the solid catalysts surface. In recent years, much efforts have been exerted to improve hetero-EF performance by constructing bimetallic Fe-based catalysts, modifying cathode with heterogeneous catalyst or introducing light illumination into hetero-EF system [34–36]. For instance, Hu et al. confirmed that the Fe/Co bimetallic nanoparticles possessed higher hetero-EF catalytic performance for organic pollutant degradation than monometallic iron compounds due to the effective Fe (II) regeneration by the reaction of Co(II) with Fe(III) [34]. Wang et al. have constructed solar heterogeneous photo-electro-Fenton (hetero--PEF) system by cathode medicated with Fe/Co bimetal MOFs/CNF catalyst to further ameliorate hetero-EF performance, and demonstrated that photoinduced electron and cathode could accelerate the redox cycles between Co(II-III-II) and Fe(II-III-II), ensuring the continual production of $^{\bullet}OH$ [35]. However, the scarcity and high toxicity of Co element limited application of Fe/Co bimetal catalysts in hetero-PEF process. Recently, many researches have verified that the $CuFeO_2$ possessed high chemical stability, well visible-light photocatalytic activity and catalytic performance for H_2O_2 activation due to its narrow band gap and cooperative impact of Fe^{3+}/Fe^{2+} and Cu^{2+}/Cu^{+} redox cycles [37–39]. Therefore, $CuFeO_2$ may be a potential hetero-PEF catalyst to modify cathode for organic pollutants degradation. Based on the superior performance of NO/PBC catalyst for H_2O_2 electrogeneration, it is hypothesized that the cathode was fabricated by the combination of $CuFeO_2$ and NO/PBC and applied in hetero-PEF system for organic pollutants degradation, which can not only realize in-situ production of $^{\bullet}OH$ through the reaction between $CuFeO_2$ and generated H_2O_2, but also accelerate the Fe^{3+}/Fe^{2+} and Cu^{2+}/Cu^{+} redox cycles under the action of photoinduced electrons and cathode. Importantly, the fabricated multifunctional cathode can effectively avoid the difficult recovery of powdered heterogeneous catalyst.

Based on the above hypothesis, the NO/PBC was prepared by pyrolysis method using alfalfa as raw material, and NO/PBC supported $CuFeO_2$ ($CuFeO_2$-NO/PBC) was prepared by hydrothermal method without additional chemical reductants. The composite gas diffusion electrodes (GDEs) were fabricated with the mixture of NO/PBC and $CuFeO_2$-NO/PBC as cathode catalyst. The NO/PBC, $CuFeO_2$-NO/PBC and composite GDEs were systematically characterized by a series of analytical methods. The hetero-PEF system was constructed with the fabricated GDEs as cathode to degrade tetracycline under visible light. The effects of key factors on tetracycline degradation were evaluated, including the NO/PBC to $CuFeO_2$-NO/PBC ratio, initial solution pH, current density and inorganic anions. The radical scavenging experiment and electron spin resonance (ESR) spectra were employed to reveal crucial reactive species for tetracycline degradation. The possible degradation pathways of tetracycline were evaluated according to intermediates. The toxicity and antibacterial property were estimated through Toxicity Estimation Software Tool (T.E.S.T.) and *Escherichia coli* growth inhibition experiments, respectively.

2. Experimental

2.1. Preparation of NO/PBC and $CuFeO_2$-NO/PBC catalyst

The NO/PBC was prepared by pyrolysis method at 500 °C using alfalfa as raw material according to previous research [29], and the detailed preparation step was recorded in Text S1. The $CuFeO_2$-NO/PBC catalyst was prepared by hydrothermal method without additional chemical reductants. Briefly, 3.6 g $Cu(NO_3)_2 \bullet 3\ H_2O$ and 6.1 g $Fe(NO_3)_3 \bullet 9\ H_2O$ were dissolved in 60 mL deionized water, then 1.0 g NO/PBC and 5.0 g NaOH were added in turn and stirred vigorously to acquire colloidal suspension. Subsequently, the suspension was poured into 100 mL Teflon-lined stainless-steel autoclave and maintained at 180 °C for 24 h. Afterwards, the obtained black precipitates were fully washed with diluted HNO_3 and deionized water, then dried at 80 °C for 8 h to acquire $CuFeO_2$-NO/PBC.

2.2. Fabrication of composite GDEs

The mixture of $CuFeO_2$-NO/PBC and NO/PBC were fully ground with different weight ratios in an agate mortar. For the fabrication of each composite GDE, 0.2 g the above mixture as cathode catalyst, 2.0 mL ethanol and 0.6 mL polytetrafluoroetylene (PTFE, 60%) emulsion as binder were stirred to gain a paste at 80 °C . The paste was completely placed onto nickel foam surface (1 ×3 cm) to form paste/nickel foam/paste with about 1.0 mm thickness. The paste/nickel foam/paste was firstly calcined at 350 °C, then soaked into dilute PTFE emulsion for 15 min and finally calcined at 300 °C to obtain composite GDEs. The weight ratios of $CuFeO_2$-NO/PBC to NO/PBC employed in the fabrication steps were 2:1, 1:1 and 0.5:1, and the corresponding composite GDEs were defined as $CuFeO_2$-NO/PBC-GDE-2.0, $CuFeO_2$-NO/PBC-GDE-1.0 and $CuFeO_2$-NO/PBC-GDE-0.5, respectively. For comparison, the $CuFeO_2$-NO/PBC-GDE and NO/PBC-GDE were fabricated using the same steps with $CuFeO_2$-NO/PBC and NO/PBC as cathode catalyst, respectively.

2.3. Characterization and electrochemical analysis

The surface morphologies of NO/PBC, $CuFeO_2$-NO/PBC and the composite GDE were characterized through scanning electron microscope (SEM) images. X-ray diffraction (XRD) spectrum was measured to investigate crystal structure of $CuFeO_2$-NO/PBC. The surface hydrophilicities of the composite GDE before and after reaction were analyzed through measuring the contact angles. X-ray photoelectron spectroscopy (XPS) analysis was used to evaluate chemical composition of $CuFeO_2$-NO/PBC. The optical and photoelectrochemical properties of $CuFeO_2$-NO/PBC were explored by UV-Vis diffuse reflectance spectrum (DRS), valence band XPS spectrum, photocurrent-time density curves and

photoluminescence (PL) spectra. The electrochemical measurements were carried out through electrochemical workstation. Graphite rob, Ag/AgCl and glassy carbon electrode loaded with catalyst were applied as counter electrode, reference electrode and working electrode, respectively. Linear sweep voltammetry (LSV) was measured through a rotating ring disk electrode (RRDE) with a Pt ring electrode in O_2-saturated solution, and the ring electrode potential was fixed 0.3 V. The electron transfer number (n) and H_2O_2 selectivity ($\%H_2O_2$) could be calculated by Eq. (5) and Eq. (6), respectively.

$$n = \frac{4 \times I_D}{I_D + \frac{I_R}{N}} \tag{5}$$

$$\%H_2O_2 = \frac{2 \times \frac{I_R}{N}}{I_D + \frac{I_R}{N}} \times 100\% \tag{6}$$

where I_D, I_R and N are the disk current (mA), the ring current (mA) and the collection efficiency (0.37), respectively.

2.4. Hetero-PEF degradation of tetracycline

The degradation performance of hetero-PEF system with composite GDEs as cathode and Pt plate as anode was assessed in an undivided quartz reactor containing 250 mL tetracycline solution and 50 mM Na_2SO_4 electrolyte under visible light. To clarify the potential and mechanism of hetero-PEF system for tetracycline degradation, 20 mg L^{-1} tetracycline was selected as target pollutant in the present work. A direct-current power and a Xe lamp with a 420 nm cut-off filter were applied to provide electric energy and visible light source, respectively. Anodic oxidation experiment of tetracycline was carried out in an undivided cell using nickel foam and Pt plate as cathode and anode, respectively. The initial solution pH was adjusted by dilute H_2SO_4 and NaOH solution. Air was pumped into electrolyte in the

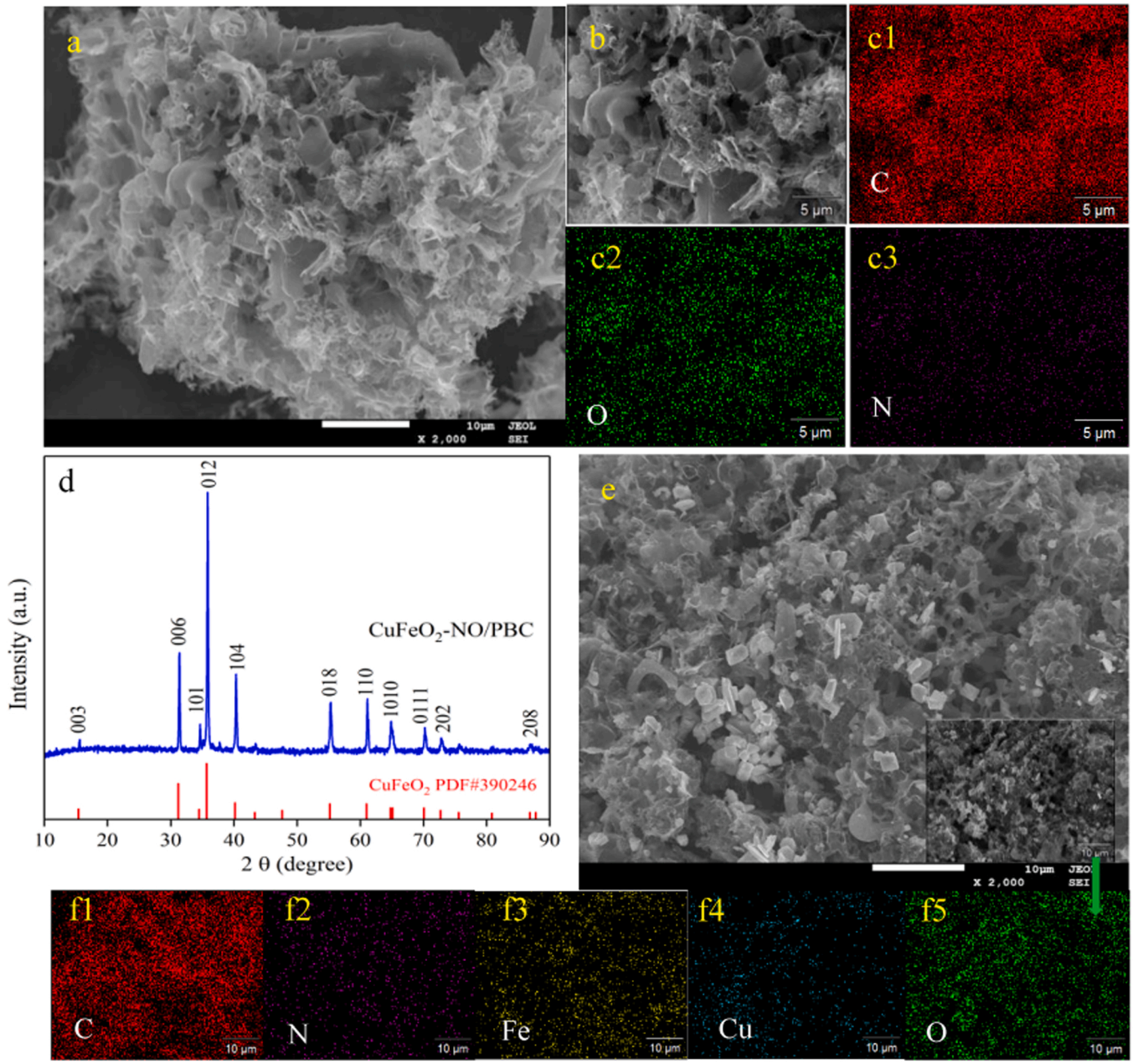

Fig. 1. The SEM images of NO/PBC (a, b) and the element maps corresponding to the SEM image (b) of NO/PBC: c1, c2, c3 were C, O and N elements, respectively. The XRD spectrum (d), SEM image (e) and the element maps of $CuFeO_2$-NO/PBC: f1, f2, f3, f4 and f5 were C, N, Fe, Cu and O elements, respectively.

vicinity of the composite GDEs during the hetero-PEF degradation process. At given time intervals, a certain amount of solution was taken out and filtered with 0.45 μm filter membranes for further analysis. The concentration of H_2O_2 and tetracycline were measured by potassium oxalate-spectrophotometric and spectrophotometric method, respectively [40]. The concentrations of leached Fe and Cu in solution were determined by an inductively coupled plasma optical emission system. The variation of total organic carbon (TOC) during hetero-PEF degradation process was monitored by a TOC analyzer. The toxicity and antibacterial property were estimated by T.E.S.T. software and *Escherichia coli* growth inhibition experiments, respectively [41].

3. Results and discussion

3.1. Characterizations of NO/PBC and $CuFeO_2$-NO/PBC

The morphology of NO/PBC was characterized by SEM image combined with element maps. The surface of NO/PBC exhibited a good 3-dimensional porous carbon structure (Fig. 1a and b) due to structural damage and loss of some functional groups from alfalfa precursor during pyrolysis process [26]. Such unique morphological feature of NO/PBC was favorable to the diffusion of O_2 in 2-electron ORR for H_2O_2 generation [29,42]. The element maps corresponding to the Fig. 1b showed a uniform distribution of C, O and N on NO/PBC surface (Fig. 1c1-c3), suggesting that the NO/PBC was successfully prepared by pyrolysis method using alfalfa as raw material.

The crystal structure of $CuFeO_2$-NO/PBC was characterized by XRD spectrum (Fig. 1d). The peaks observed at 15.7°, 31.4°, 34.7°, 35.9°, 40.4°, 55.4°, 61.2°, 64.9°, 70.3°, 72.9° and 86.9° were respectively relevant to Bragg reflections from the (003), (006), (101), (012), (104), (018), (110), (1010), (0111) (202) and (208) crystalline planes of $CuFeO_2$ (PDF#390246), and no other impurity phases were observed, which indicated that $CuFeO_2$-NO/PBC containing pure-phase $CuFeO_2$ could be prepared by hydrothermal method. The $CuFeO_2$ particles were predominantly deposited onto the NO/PBC surface and embedded in 3-dimensional porous carbon structure (Fig. 1e), which was conducive to

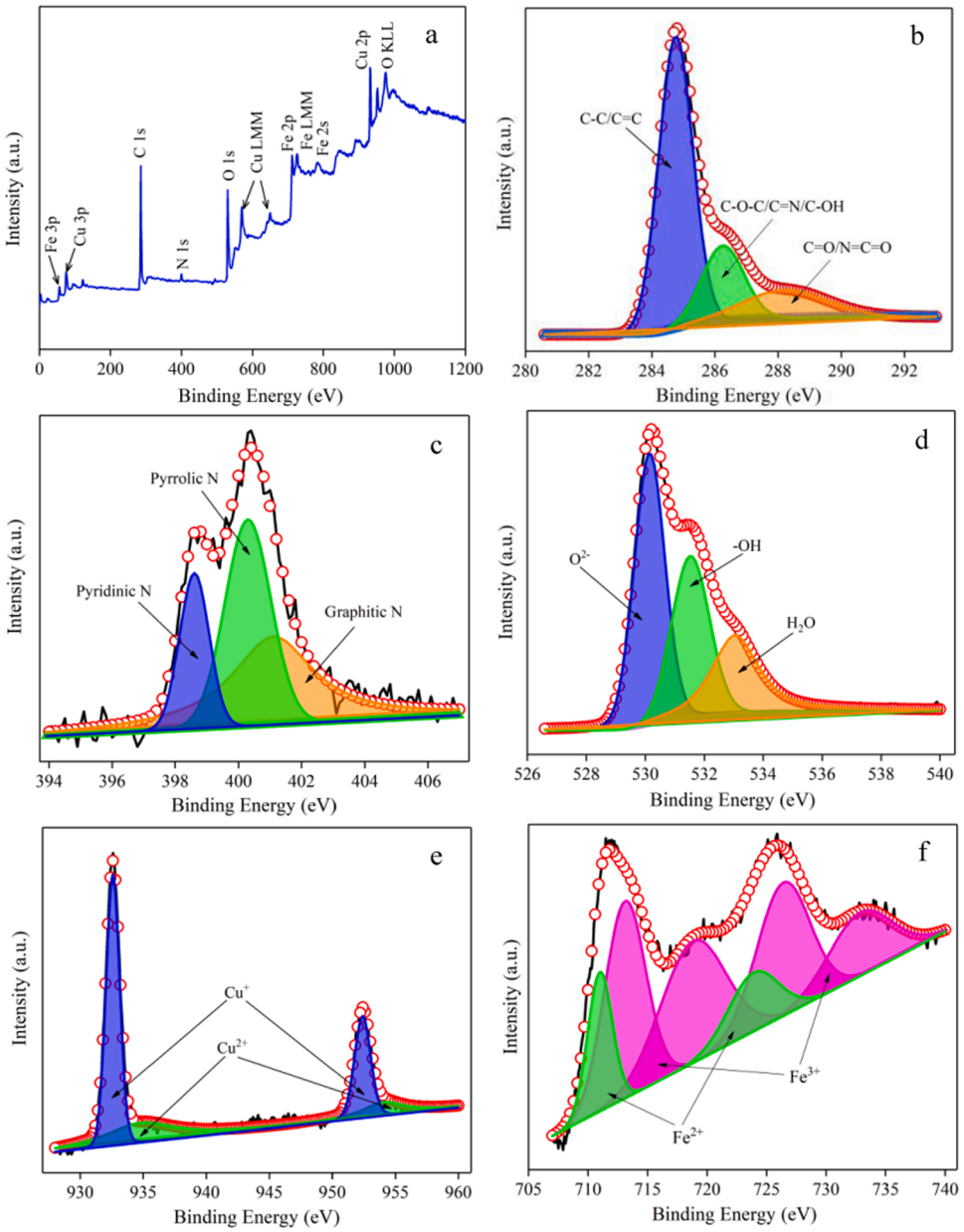

Fig. 2. Surface survey XPS spectrum (a), C 1s (b), N 1s (c), O 1 (d), Cu 2p (e) and Fe 2p (f) high-resolution XPS spectra of $CuFeO_2$-NO/PBC.

alleviate the agglomeration of $CuFeO_2$ particles. The element maps corresponding to the inset of Fig. 1e displayed that C, N, Fe, Cu and O elements were homogenously distributed on $CuFeO_2$-NO/PBC surface (Fig. 1f1-f5). The presence of these five elements could be also demonstrated by the surface survey XPS spectrum of $CuFeO_2$-NO/PBC (Fig. 2a). The C 1s high-resolution XPS spectrum (Fig. 2b) could be resolved into three dominant peaks at 284.76 eV, 286.25 eV and 288.19 eV, which were assigned to C-C/C═C, C–O-C/C═N/C-OH and C═O/N═C═O, respectively. In the N 1 s high-resolution XPS spectrum of $CuFeO_2$-NO/PBC (Fig. 2c), three signals at 398.6 eV, 400.3 eV and 401.1 eV were respectively corresponded to pyridinic N, pyrrolic N and graphitic N, which further suggest the existence of N functional groups. Previous researches have confirmed that C-O-C, pyrrolic N and graphitic N were active sites for H_2O_2 generation through 2-electron ORR [23,43,44]. The O 1 s high-resolution XPS spectrum could be separated to three dominant bonds at 530.2 eV, 531.9 eV and 533.7 eV (Fig. 2d), which were attributed to lattice oxygen (O^{2-}) in $CuFeO_2$, -OH and H_2O, respectively. The Cu 2p and Fe 2p high-resolution XPS spectra of $CuFeO_2$-NO/PBC were shown in Fig. 2e and f. The Cu^+ was identified by the signals at 932.6 eV and 952.4 eV, and other two weak signals at higher binding energies of Cu 2p were ascribed to Cu^{2+}. The signals at 713.1 eV and 724.4 eV with two satellite peaks at 718.8 eV and 732. 8 eV were corresponded to Fe^{3+}, and the weak Fe^{2+} signals were located at 711.0 eV and 723.9 eV. The present results indicated that the valence states of Cu and Fe were + 1 and + 3, respectively. The UV-Vis DRS and $(\alpha h\nu)^2$-hν curve (Fig. S1) showed that $CuFeO_2$-NO/PBC possessed good visible-light response and its calculated bandgap was 2.35 eV. In the valence band XPS spectrum (Fig. S2), the valence band potential of $CuFeO_2$-NO/PBC was 1.48 eV, thus the conduction band potential could be calculated as 0.87 eV. In addition, photocurrent-time density curve and PL spectra were investigated under visible light and dark to further explore the photocatalytic performance of $CuFeO_2$-NO/PBC. The photocurrent density of $CuFeO_2$-NO/PBC had a significant increase after introducing visible light (Fig. 3a). The PL spectra of $CuFeO_2$-NO/PBC appeared an excitation peak under visible light, while no excitation peak was observed under dark (Fig. 3b), indicating that $CuFeO_2$-NO/PBC could undergo the transfer and recombination of photoinduced electron-hole pairs [41]. The above results demonstrated that $CuFeO_2$-NO/PBC owned potential visible light catalytic activity.

The electrocatalytic behaviors of NO/PBC and $CuFeO_2$-NO/PBC for ORR were further investigated through measuring ring current and disk current from LSV in O_2-saturated solution. The limiting disk current and disk onset potential of ORR for NO/PBC were higher than that for $CuFeO_2$-NO/PBC (Fig. 3c), which might be explained that numerous $CuFeO_2$ particles was attached to NO/PBC surface, masking the active sites responsible for ORR. The calculated electron transfer numbers for NO/PBC and $CuFeO_2$-NO/PBC were between 2 and 4 (Fig. S3), implying that NO/PBC and $CuFeO_2$-NO/PBC could induce ORR through 2-electron and 4-electron pathways [19]. Fig. 3d displayed that the highest H_2O_2 selectivity of NO/PBC and $CuFeO_2$-NO/PBC were 85.5% and 52.3%, respectively. The relatively low H_2O_2 selectivity of $CuFeO_2$--NO/PBC might be attributed to that $CuFeO_2$ on the NO/PBC surface could mask partial active sites for H_2O_2 electrogeneration and accelerate the decomposition of H_2O_2 to produce reactive oxygen species.

3.2. Tetracycline degradation in different systems

The degradation efficiency and apparent rate constant of tetracycline were investigated in different systems to assess the performance of hetero-PEF system. Fig. 4a showed that the adsorption removal rate of tetracycline by $CuFeO_2$-NO/PBC-GDE-1.0 as a typical GDE was negligible due to that the PTFE coating evenly covered on the $CuFeO_2$-NO/PBC-GDE-1.0 surface caused its good hydrophobic property (Fig. S4). The tetracycline degradation efficiency by $CuFeO_2$-NO/PBC-GDE-1.0 in photocatalytic system was 17.4% at pH 5.0 after 180 min, which was only 2.3% higher than that by photolysis under visible light. The phenomenon can be clarified as low valence band potential of $CuFeO_2$-NO/PBC (Fig. S2) and good surface hydrophobic property of $CuFeO_2$-NO/

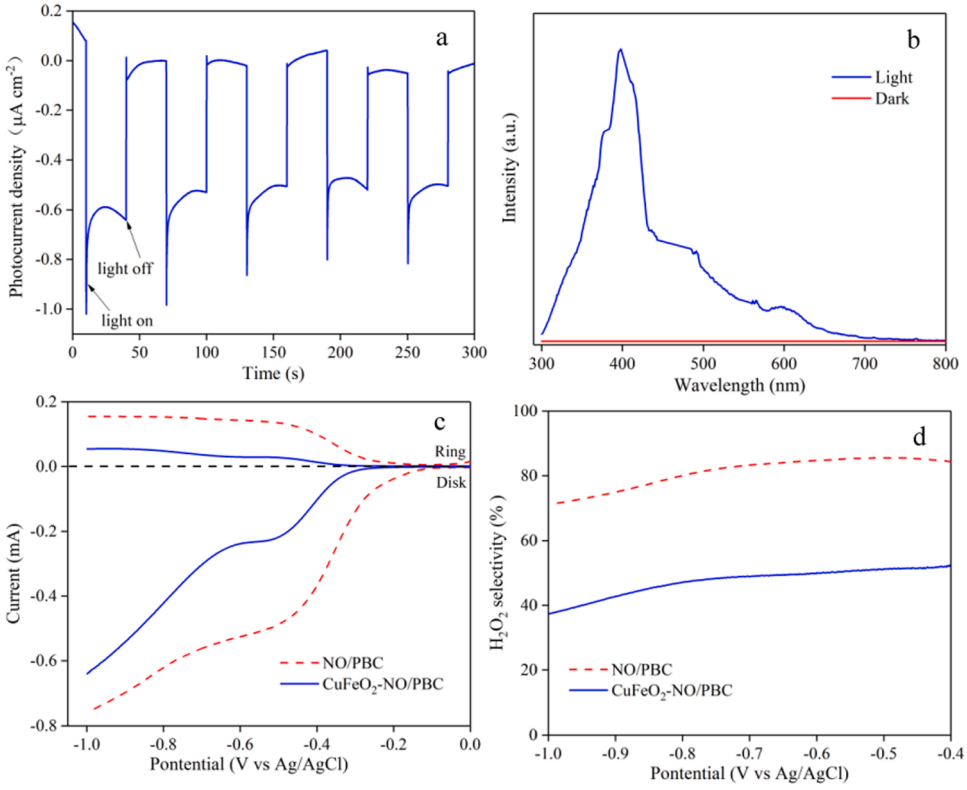

Fig. 3. Photocurrent-time curve (a), PL spectra (b) of $CuFeO_2$-NO/PBC under light and dark, ring current and disk current of RRDE measurement at 5 mV s^{-1} and 1600 rpm (c) and H_2O_2 selectivity (d) of NO/PBC and $CuFeO_2$-NO/PBC in O_2-saturated solution.

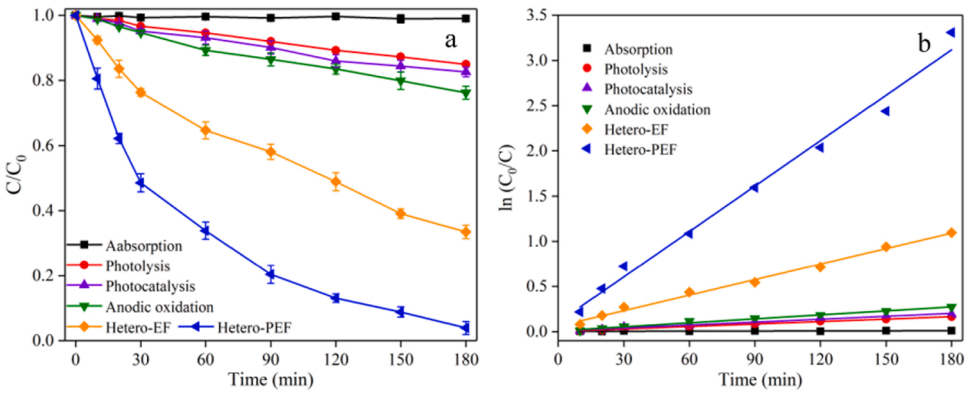

Fig. 4. Degradation (a) and corresponding kinetic curves (b) of tetracycline in different systems. ($CuFeO_2$-NO/PBC-GDE-1.0 as cathode, [current density]$_0$ = 80 mA cm^{-2}, [tetracycline]$_0$ = 20 mg L^{-1} and pH = 5.0).

PBC-GDE-1.0 (Fig. S4). For the hetero-EF system, approximately 66.5% tetracycline was removed within 180 min using $CuFeO_2$-NO/PBC-GDE-1.0 as cathode, which was higher than the anodic oxidation efficiency (25.1%) of tetracycline by Pt plate anode, indicating that $CuFeO_2$-NO/PBC-GDE-1.0 as cathode could produce more active radicals to degrade tetracycline. After introducing visible light, the tetracycline degradation efficiency in hetero-PEF system could be significantly improved to 96.1% after 180 min. According to pseudo-first-order kinetics model (Fig. 4b), the apparent rate constant (0.01674 min^{-1}) of hetero-PEF system for tetracycline degradation was higher than those of hetero-EF system (0.00573 min^{-1}), anodic oxidation (0.00147 min^{-1}) and photocatalysis system (0.00108 min^{-1}), which further demonstrated fine degradation performance of hetero-PEF system.

3.3. Effect of key factors on tetracycline degradation in hetero-PEF system

3.3.1. Effect of NO/PBC to $CuFeO_2$-NO/PBC ratio on tetracycline degradation

The NO/PBC and $CuFeO_2$-NO/PBC could be used as cathode catalyst to produce H_2O_2 through 2-electron ORR and activate H_2O_2 for active radical generation, respectively. Therefore, the effect of NO/PBC to $CuFeO_2$-NO/PBC ratio on tetracycline degradation was investigated using composite GDEs with NO/PBC, $CuFeO_2$-NO/PBC and different NO/PBC to $CuFeO_2$-NO/PBC ratios mixture as cathode catalyst in hetero-PEF system. Although the H_2O_2 accumulation with NO/PBC-GDE as cathode was the highest compared with other composite GDEs (Fig. S5), the tetracycline degradation efficiency was 51.7% in hetero-PEF system using NO/PBC-GDE cathode (Fig. 5a and Table S1) due to that the lack of $CuFeO_2$-NO/PBC caused ineffective H_2O_2 activation. The

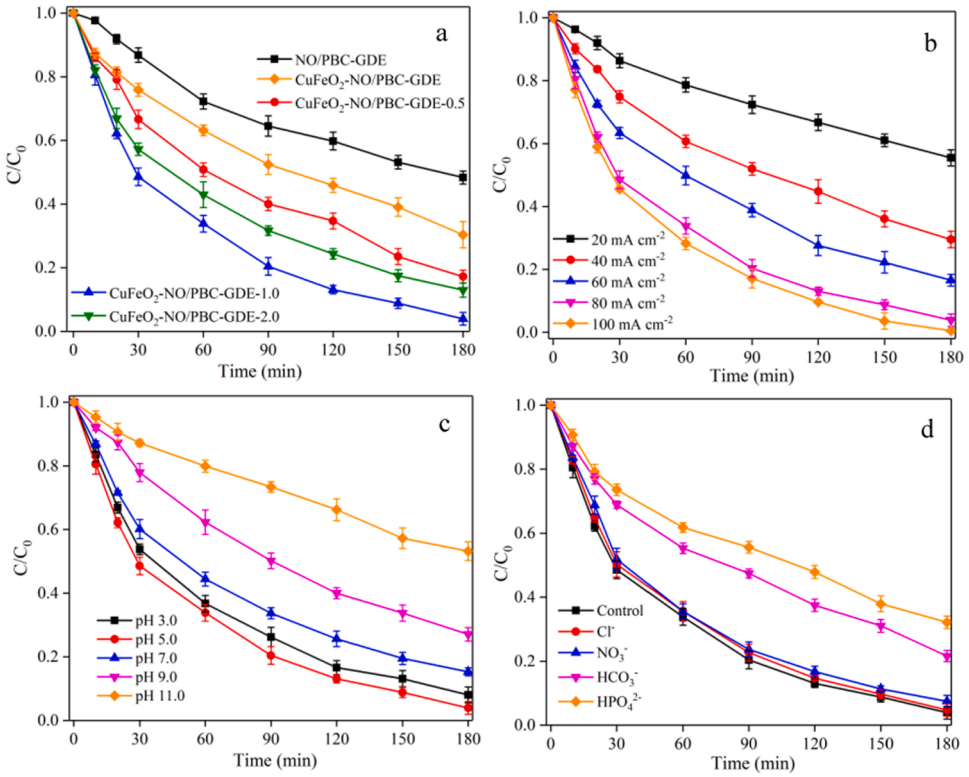

Fig. 5. Effect of NO/PBC to $CuFeO_2$-NO/PBC ratio (a), current density (b), solution pH (c) and inorganic anions (d) on tetracycline degradation (Except for the investigated factors, the others were fixed on NO/PBC to $CuFeO_2$-NO/PBC ratio of 1:1, [current density]$_0$ = 80 mA cm^{-2}, [tetracycline]$_0$ = 20 mg L^{-1}, pH = 5.0 and [inorganic anions]$_0$ =10 mM).

tetracycline degradation efficiency was 69.6% in hetero-PEF system using $CuFeO_2$-NO/PBC-GDE cathode (Fig. 5a and Table S1), which can be explained by the lowest H_2O_2 electrogeneration (Fig. S5). The $CuFeO_2$-NO/PBC-GDE-x (x = 0.5, 1.0, 2.0) exhibited higher tetracycline degradation efficiency than NO/PBC-GDE and $CuFeO_2$-NO/PBC-GDE, and the tetracycline degradation efficiencies were 82.8%, 96.1% and 87.0% with $CuFeO_2$-NO/PBC-GDE-0.5, $CuFeO_2$-NO/PBC-GDE-1.0 and $CuFeO_2$-NO/PBC-GDE-2.0 as cathode, respectively (Fig. 5a and Table S1), which was related to the H_2O_2 accumulation trend (Fig. S5). Likewise, the apparent rate constant for tetracycline degradation by $CuFeO_2$-NO/PBC-GDE-1.0 based on pseudo-first-order kinetics model (Fig. S6) was higher than those by other as-fabricated GDEs in the present work (Table S1). The present results demonstrated the mixture of NO/PBC and $CuFeO_2$-NO/PBC as cathode catalyst could not only generate sufficient H_2O_2, but also activate H_2O_2 to produce more active radicals for tetracycline degradation. According to the above results, the $CuFeO_2$-NO/PBC-GDE-1.0 with NO/PBC to $CuFeO_2$-NO/PBC ratio of 1:1 was chosen as a most optimized composite GDE in hetero-PEF system for tetracycline degradation.

3.3.2. Effect of current density on tetracycline degradation

The current density is a critical factor affecting H_2O_2 electorgeneration, which can determine active radical generation in EF-based technique [11]. To evaluate the effect of current density on tetracycline degradation in hetero-PEF system, degradation experiments were carried out with $CuFeO_2$-NO/PBC-GDE-1.0 as cathode (Fig. 5b). The tetracycline degradation efficiency heightened from 44.5% at 20 mA cm^{-2} to 96.1% at 80 mA cm^{-2} after 180 min, which corresponded to the H_2O_2 accumulation trend by increasing current density (Fig. S7). Although the accumulation of H_2O_2 continued to increase as current density was further increased to 100 mA cm^{-2}, no obvious increase in the tetracycline degradation efficiency was obtained as a result of the scavenging effect of $^{\bullet}OH$ by H_2O_2 (Eqs. 7–8) [34,45]. The formed $^{\bullet}O_2H$ and $\bullet O_2^-$ had weaker oxidation activity than $^{\bullet}OH$, which was detrimental to tetracycline degradation. Additionally, several competitive reactions including 4-electron ORR and hydrogen evolution reaction could be promoted at 100 mA cm^{-2}, which limited the degradation performance of hetero-PEF system.

$$\bullet OH + H_2O_2 \rightarrow H_2O + \bullet O_2H \quad (7)$$

$$\bullet O_2H \leftrightarrow \bullet O_2^- + H^+ \quad (8)$$

3.3.3. Effect of initial solution pH on tetracycline degradation

The solution pH from 3.0 to 11.0 on tetracycline degradation was evaluated in hetero-PEF system. The tetracycline degradation efficiency declined from 96.1% at pH 5.0 to 84.7% at pH 7.0, 72.9% at pH 9.0% and 46.8% pH 11.0 after 180 min (Fig. 5c), which might be related to the H_2O_2 electrogeneration under different pH conditions. The H_2O_2 accumulation in solution was investigated using $CuFeO_2$-NO/PBC-GDE-1.0 as cathode without light (Fig. S8), and the H_2O_2 accumulation in solution decreased respectively from 278.9 mg L^{-1} to 244.7 mg L^{-1} and 224.7 mg L^{-1} with the solution pH from 5.0 to 7.0 and 9.0 after 180 min, demonstrating that adequate H^+ at pH 5.0 could be available for H_2O_2 electrogeneration through 2-electron ORR (Eq. 1). Although the concentration of H^+ in the solution at pH 7.0 and pH 9.0 were slightly insufficient for H_2O_2 electrogeneration, H^+ continuously generated at anode by Eq. 9 could also participate in H_2O_2 electrogeneration [29]. Moreover, the existence of enough H^+ at low solution pH could promote $^{\bullet}OH$ production (Eq. 10) using Cu-Fe bimetallic catalyst for H_2O_2 activation and was conducive to tetracycline degradation [6]. However, the H_2O_2 accumulation significantly decreased to 28.5 mg L^{-1} at pH 11.0 after 180 min, which suggested that excessive OH^- in the solution was detrimental to H_2O_2 electrogeneration and accelerated H_2O_2 decomposition. The H_2O_2 accumulation increased to 314.1 mg L^{-1} at pH 3.0, while the inhibition of tetracycline degradation efficiency was observed in hetero-PEF system. This phenomenon can be explained as the capture of $^{\bullet}OH$ by excess H^+ at pH 3.0 (Eq. 11). In addition, the tetracycline existent form (H_3TC^+) at pH 3.0 was not vulnerable to attack by reactive oxygen species compared with the formed H_2TC^0 at pH 5.0 as a result of lower electron densities in H_3TC^+ ring than that in H_2TC^0 ring.

$$2H_2O\text{-}4e^- \rightarrow 4H^+ + O_2 \quad (9)$$

$$\equiv Cu^+/Fe^{2+} + H_2O_2 + H^+ \rightarrow \equiv Cu^{2+}/Fe^{3+} + H_2O + HO^{\bullet} \quad (10)$$

$$H^+ + HO^{\bullet} + e^+ \rightarrow H_2O \quad (11)$$

3.3.4. Effect of dissolved anions on tetracycline degradation

The coexistence of some typical dissolved anions (e.g., Cl^-, NO_3^-, HCO_3^- and HPO_4^{2-}) in the practical water containing target pollutant may affect the degradation performance of hetero-PEF system. Compared to the control without anions (Fig. 5d), the Cl^- had no inhibitory effect on tetracycline degradation. Although Cl^- could quench $^{\bullet}OH$ to produce a transient intermediate ($ClOH^{\bullet-}$) through Eq. 12 with rate constant of 4.3 $\pm$ 0.4 $\times$ 10^9 M^{-1} s^{-1}, the $^{\bullet}OH$ regeneration could be realized quickly through the decomposition of $ClOH^{\bullet-}$ with rate constant of 6.1 $\pm$ 0.8 $\times$ 10^9 M^{-1} s^{-1} (Eq. 13) [46]. It is reported that NO_3^- is a common photosensitizer [47], whereas NO_3^- was hardly apparent effect on tetracycline degradation. Due to the low molar absorption coefficient of NO_3^- under visible light, the production of $^{\bullet}OH$ was limited through the photolysis of NO_3^- [47]. The NO_3^- could not effectively capture $HO^{\bullet}$ as a result of low reaction rate between $^{\bullet}OH$ and NO_3^- [48]. Previous research has claimed that the complexation of NO_3^- with powder catalyst could affect H_2O_2 activation on the catalyst surface [41], whereas the NO_3^- may not complex with $CuFeO_2$-NO/PBC due to good surface hydrophobic property of $CuFeO_2$-NO/PBC-GDE-1.0 (Fig. S4) in the present work. The tetracycline degradation efficiency declined from 96.1% of the control (no anions) to 78.4% and 67.8% when HCO_3^- and HPO_4^{2-} were introduced into hetero-PEF system, respectively. The present results can be explained that HCO_3^- and HPO_4^{2-} could react with $^{\bullet}OH$ to produce lower effective $CO_3^{\bullet-}$ and $HPO_4^{\bullet-}$ (Eqs. 14–15), which inhibited tetracycline degradation.

$$Cl^- + HO^{\bullet} \rightarrow ClOH^{\bullet-} \quad (12)$$

$$ClOH^{\bullet-} \rightarrow Cl^+ + HO^{\bullet} \quad (13)$$

$$HCO_3^- + HO^{\bullet} \rightarrow CO_3^{\bullet-} + H_2O \quad (14)$$

$$HPO_4^{2-} + HO^{\bullet} \rightarrow HPO_4^{\bullet-} + OH^- \quad (15)$$

3.4. Reusability and stability

To evaluate the performance of hetero-PEF system for tetracycline degradation under long-term operation, H_2O_2 accumulation in solution by $CuFeO_2$-NO/PBC-GDE-1.0 cathode and tetracycline degradation at hetero-PEF system for 5 recycling experiments were performed at 80 mA cm^{-2} and pH 5.0. The H_2O_2 accumulation in solution decreased from 285.6 to 253.3 mg L^{-1} without light after 5 recycling experiments (Fig. 6a), which confirmed that $CuFeO_2$-NO/PBC-GDE-1.0 exhibited good reusability. Fig. 6b displayed that the tetracycline degradation efficiency in hetero-PEF system could still reach more than 80% after five cycles (900 min), indicating that hetero-PEF system had good stability for tetracycline degradation. In addition, the contact angle between $CuFeO_2$-NO/PBC-GDE-1.0 and water diminished from the initial 126.3° (Figs. 6c) to 120.5° (Fig. 6d) after 5 cycles in hetero-PEF system, and the concentrations of leached Fe and Cu in solution were hardly detected after 180 min, which have further demonstrated the stability of hetero-PEF system using $CuFeO_2$-NO/PBC-GDE-1.0 for tetracycline

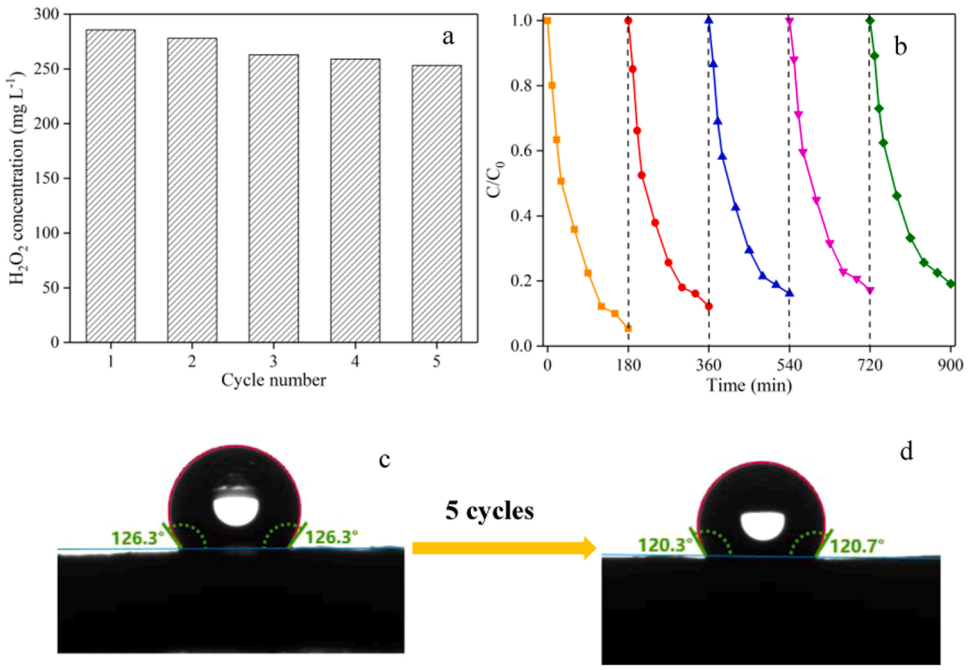

Fig. 6. Accumulation of H_2O_2 produced in solution by $CuFeO_2$-NO/PBC-GDE-1.0 without light for 5 consecutive experiments (a), recycling degradation of tetracycline in hetero-PEF system (b), the contact angles of $CuFeO_2$-NO/PBC-GDE-1.0 (c) and $CuFeO_2$-NO/PBC-GDE-1.0 after 5 cycles (d) ([current density]$_0$ = 80 mA cm^{-2}, [tetracycline]$_0$ = 20 mg L^{-1} and pH = 5.0).

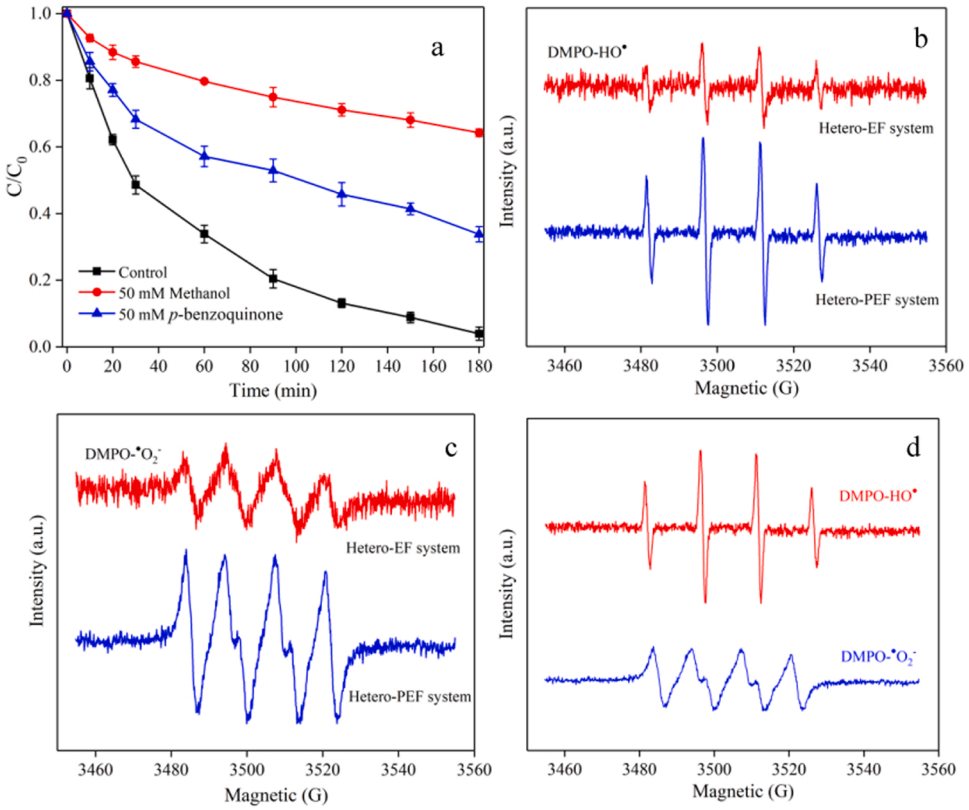

Fig. 7. Effect of various radical scavengers on tetracycline degradation in hetero-PEF system (a), ESR spectra of DMPO-•OH (b) and DMPO-•O_2^- (c) in hetero-EF and hetero-PEF systems. ESR spectra (d) of DMPO-•OH and DMPO-•O_2^- at the same reaction time in hetero-PEF systems ([tetracycline]$_0$ =20 mg L^{-1}, [current density]$_0$ =80 mA cm^{-2} and pH=5.0).

degradation under long-term operation.

3.5. Reactive species and proposed mechanism

3.5.1. Reactive species identification

As the crucial reactive species for Fenton-based system, the $^{\bullet}OH$ and $^{\bullet}O_2^-$ can be continuously produced by activating H_2O_2 with heterogeneous catalyst for organic contaminants degradation. Therefore, excessive methanol (50 mM) and *p*-benzoquinone (50 mM) were used as scavengers to quench $^{\bullet}OH$ and $^{\bullet}O_2^-$, respectively [6]. Fig. 7a displayed that the tetracycline degradation efficiency declined from 96.1% of the control (no scavenger) to 35.8% in the presence of methanol. However, the tetracycline degradation efficiency was only declined to 66.2% when *p*-benzoquinone was added into hetero-PEF system, suggesting that $^{\bullet}OH$ and $^{\bullet}O_2^-$ played the primary and auxiliary roles for tetracycline degradation during the hetero-PEF process, respectively. The ESR/DMPO experiments were performed for further identifying active radical production in hetero-EF and hetero-PEF system. As shown in Fig. 7b and c, the 1:2:2:1 quadruplet signal of DMPO-$^{\bullet}OH$ and the 1:1:1:1 quadruplet signal of DMPO- $^{\bullet}O_2^-$ were detected in hetero-EF and hetero-PEF system [38], which confirmed that $CuFeO_2$-NO/PBC-GDE-1.0 as cathode could not only produce H_2O_2 through 2-electron ORR, but also activate H_2O_2 to form $^{\bullet}OH$ and $^{\bullet}O_2^-$. Compared with hetero-EF system, the signal intensities of DMPO-$^{\bullet}OH$ and DMPO-$^{\bullet}O_2^-$ obviously increased in hetero-PEF system, demonstrating that the visible light could promote the production of $^{\bullet}OH$ and $^{\bullet}O_2^-$. Moreover, the signal intensity of DMPO-$^{\bullet}OH$ was stronger than that of DMPO-$^{\bullet}O_2^-$ at the same reaction time in hetero-PEF system (Fig. 7d). The present result confirmed that the contribution of $^{\bullet}OH$ for tetracycline degradation was higher than that of $^{\bullet}O_2^-$ in hetero-PEF system, consisting with the experimental results of active species capture.

3.5.2. Proposed mechanism

In hetero-PEF system, air was blown externally onto $CuFeO_2$-NO/PBC-GDE-1.0 surface and diffused to the active site of $CuFeO_2$-NO/PBC through the three-phase interface. Previous research has confirmed that the adsorption energy of OOH (a unique intermediate for the 2-electron ORR) on graphitic N, the co-doping of graphitic N and C-O-C, and the co-doping of pyrrolic N and C-O-C in NO/PBC was lower than that on pure carbon substrate based on density functional theory calculation [29], which could reduce oxygen in the air to H_2O_2 by 2-electron ORR. The generated H_2O_2 activation mainly occurred through catalyst surface reaction containing both Fe and Cu sites since the concentrations of leached Cu and Fe in solution were hardly measured after 180 min in hetero-PEF system. To reveal the possible mechanism of H_2O_2 activation by $CuFeO_2$ on $CuFeO_2$-NO/PBC-GDE-1.0 surface, XPS analysis was carried out to estimate the valence states and contents of Cu and Fe before and after degradation. From the Fe 2p high-resolution XPS spectra (Fig. S9), the Fe^{3+} content reduced from 84.6% to 82.2% with the increase of Fe^{2+} content from 15.4% to 17.8% after degradation. The Cu 2p high-resolution XPS spectra (Fig. S10) showed that the relative contents of the Cu^+ and Cu^{2+} species were 91.5% and 8.5%, respectively. The content of Cu^{2+} increased to 15.3% after degradation, while the Cu^+ content decreased to 84.7%. The Fe^{3+}/Fe^{2+} content ratio and Cu^{2+}/Cu^+ content ratio on the catalyst surface had changed after degradation, indicating that Fe and Cu species participated in hetero-PEF reaction. Fig. 8 showed the mechanism scheme of tetracycline hetero-PEF degradation by $CuFeO_2$-NO/PBC-GDE-1.0. During the degradation reaction process, the $\equiv Fe^{3+}$ on $CuFeO_2$ surface could be reduced to $\equiv Fe^{2+}$ and $^{\bullet}O_2^-$ by H_2O_2 via intramolecular electron transfer (Eq. 16), the formed $\equiv Fe^{2+}$ reacted with H_2O_2 to produce $^{\bullet}OH$ in the light of Haber-Weiss mechanism (Eq. 17). Similarly, the $\equiv Cu^+$ on $CuFeO_2$ surface reacted with H_2O_2 to produce $^{\bullet}OH$ (Eq. 18), and the $\equiv Cu^{2+}$ was reduced to Cu^+ via reaction with H_2O_2 and produce $^{\bullet}O_2^-$ (Eq. 19). In addition, the reduction of $\equiv Fe^{3+}$ by $\equiv Cu^+$ to $\equiv Fe^{2+}$ by thermodynamically favorable electron transfer was acquired (Eq. 20) as a result of lower redox potential of Cu^{2+}/Cu^+ (0.17 V) than Fe^{3+}/Fe^{2+} (0.77 V) [49,50]. Simultaneously, the electron on the cathode surface could react with $\equiv Fe^{3+}$ and $\equiv Cu^{2+}$ to generate $\equiv Fe^{2+}$ and $\equiv Cu^+$ to achieve catalyst circulation (Eq.21), which promoted tetracycline degradation in hetero-EF system.

$$\equiv Fe^{3+} + H_2O_2 \rightarrow \equiv Fe^{2+} + O_2^{\bullet-} + 2H^+ \quad (16)$$

$$\equiv Fe^{2+} + H_2O_2 \rightarrow \equiv Fe^{3+} + HO^{\bullet} + OH^- \quad (17)$$

$$\equiv Cu^{+} + H_2O_2 \rightarrow \equiv Cu^{2+} + HO^{\bullet} + OH^- \quad (18)$$

$$\equiv Cu^{2+} + H_2O_2 \rightarrow \equiv Cu^{+} + O_2^{\bullet-} + 2H^+ \quad (19)$$

$$\equiv Fe^{3+} + \equiv Cu^{+} \rightarrow \equiv Fe^{2+} + \equiv Cu^{2+} \quad (20)$$

$$\equiv Fe^{3+}/\equiv Cu^{+} + e^-(\text{cathode}) \rightarrow \equiv Fe^{2+}/\equiv Cu^{+} \quad (21)$$

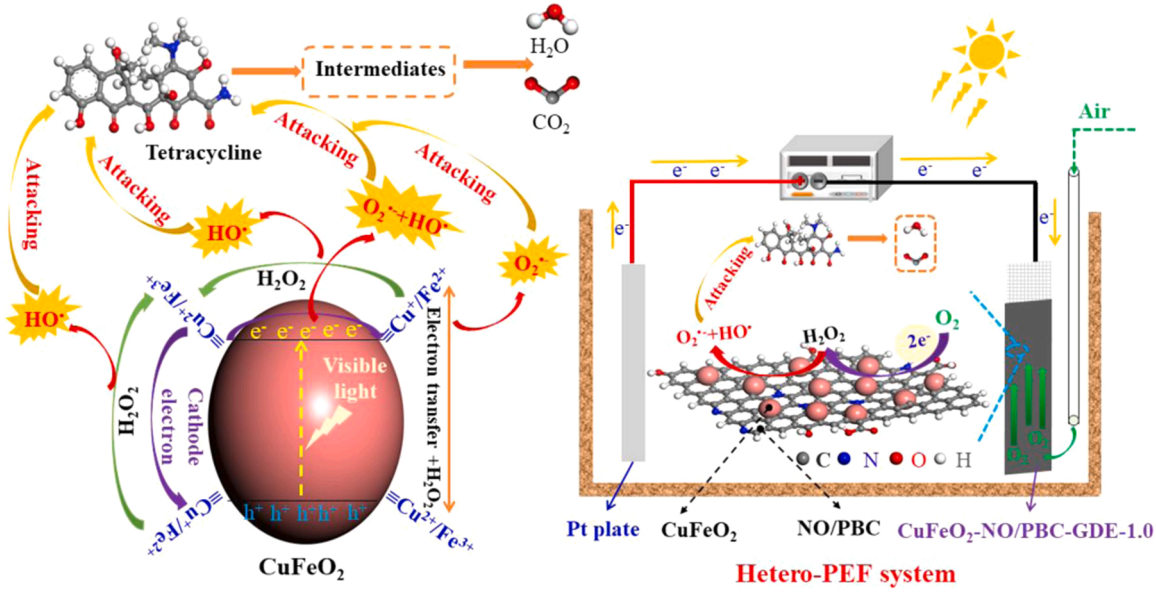

Fig. 8. Proposed mechanism scheme for tetracycline degradation in hetero-PEF system.

The promotion of tetracycline degradation, and the increase in the signal intensities of DMPO-$^{\bullet}$OH and DMPO-$^{\bullet}O_2^-$ were observed in hetero-PEF system compared with those in hetero-EF system, indicating that $CuFeO_2$-NO/PBC as cathode could improve the performance of hetero-EF system by introduction of visible light. The $CuFeO_2$-NO/PBC could be excited under visible light to generate photoinduced hole and electron (Eq. 22). The photoinduced hole could not effectively degrade tetracycline (Fig. 4a) due to the fact that the valence band potential (1.48 eV) of $CuFeO_2$-NO/PBC (Fig. S2) was lower than + 2.4 eV ($^{\bullet}$OH/OH^-) and + 2.72 eV ($^{\bullet}$OH/H_2O). However, the photoinduced electron not only reacted with H_2O_2 and O_2 to form $^{\bullet}$OH and $^{\bullet}O_2^-$ (Eqs. 23–24), but also promoted in-situ recycling of $\equiv Fe^{2+}$ to $\equiv Fe^{2+}$ and $\equiv Cu^{2+}$ to $\equiv Cu^{+}$ (Eq. 25), which was beneficial for active species generation. Moreover, the H_2O_2 in solution was also decomposed into $^{\bullet}$OH by direct photolysis (Eq. 26), and then the tetracycline could be converted into degradation products by formed reactive species ($^{\bullet}$OH/$^{\bullet}O_2^-$) (Eq. 27).

$$CuFeO_2\text{-NO/PBC} + \text{visible light} \rightarrow h^+ + e^- \quad (22)$$

$$e^- + H_2O_2 \rightarrow HO^{\bullet} + OH^- \quad (23)$$

$$e^- + O_2 \rightarrow O_2^{\bullet -} \quad (24)$$

$$\equiv Fe^{3+}/\equiv Cu^{2+} + e^- \rightarrow \equiv Fe^{2+}/\equiv Cu^{+} \quad (25)$$

$$h\nu + H_2O_2 \rightarrow 2HO^{\bullet} \quad (26)$$

$$HO^{\bullet}/O_2^{\bullet -} + \text{tetracycline} \rightarrow \text{intermediates} \rightarrow CO_2 + H_2O \quad (27)$$

3.6. Degradation intermediates and toxicity analysis

To illustrate the hetero-PEF degradation process of tetracycline by $CuFeO_2$-NO/PBC-GDE-1.0, the HPLC/MS analysis was adopted for identifying degradation intermediates. According to the HPLC/MS spectra (Fig. S11), the possible degradation pathways of tetracycline were shown in Fig. 9. Tetracycline organic fragment (m/z = 445) was transformed into fragment P1 (m/z 431) by detachment of methyl group due to the low N–C bond energy [51]. The formed P1 was converted to fragment P5 (m/z 402) by the loss of amino group and methyl group under the continuous attack of active radicals. Furthermore, the fragment P2 (m/z = 427) came from tetracycline degradation through dehydration reaction. The cleavage of the third ring in P2 and hydroxylation reaction under attack of active radicals could further result in formation of fragments P3 (m/z = 231) and P4 (m/z = 249) [52]. The loss of amino group and methyl group from P2 formed fragment P6 (m/z = 369), and the P6 was also produced by the loss amino group and H_2O from P5. The fragment P7 (m/z = 321) was produced by cracking the fourth ring and removing amino groups from P5 under attack of active radicals, and the formed P7 was converted into P8 (m/z = 281) through the fracture of the third ring and double carbon bonds. The P4, P6 and P8 was transformed to the fragment P9 (m/z = 181) by the second ring crack, dehydration and hydroxylation reaction. Subsequently, the fragment P10 (m/z = 169) was produced by open-ring reaction, demethylation and hydroxylation from P4, and also was formed through demethylation from P9. The formed partial intermediates were further degraded to CO_2 and H_2O under free radical attack.

The T.E.S.T. software was used to estimate the toxicity of tetracycline and its intermediates after hetero-PEF degradation by $CuFeO_2$-NO/PBC-GDE-1.0 cathode. As displayed in Fig. 10a, the lethal concentration of 50% Daphnia magna (LC_{50}-48 h) of tetracycline was 8.7 mg L^{-1}, indicating that tetracycline was a "toxic" pollutant. The LC_{50}-48 h of P3 (140.7 mg L^{-1}), P7 (18.4 mg L^{-1}), P8 (59.6 mg L^{-1}), P9 (75.6 mg L^{-1}) and P10 (191.8 mg L^{-1}) were higher than 10 mg L^{-1}, thus these intermediates was defined as "harmful" pollutants for Daphnia magna.

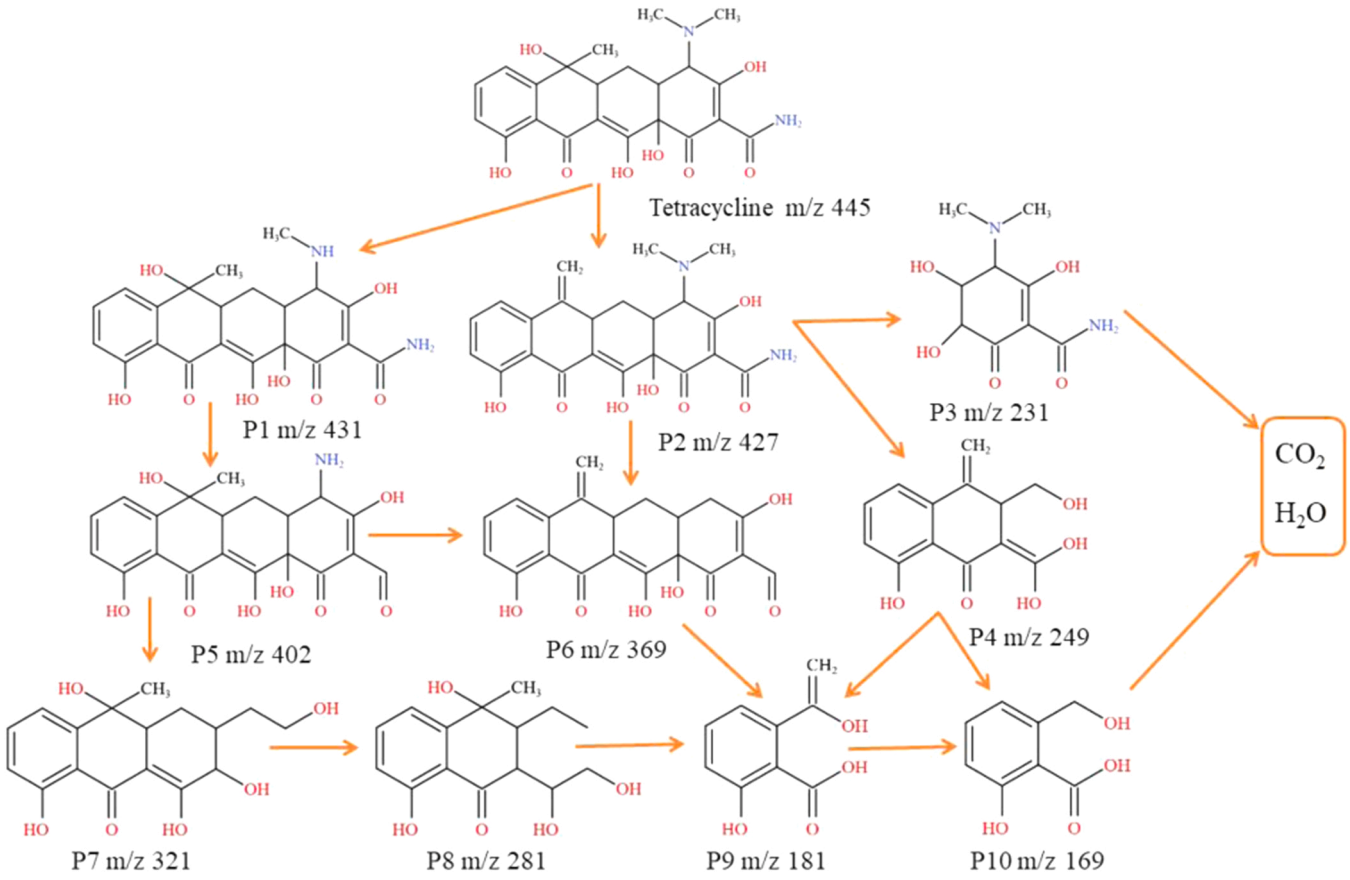

Fig. 9. Proposed degradation pathway of tetracycline in hetero-PEF system.

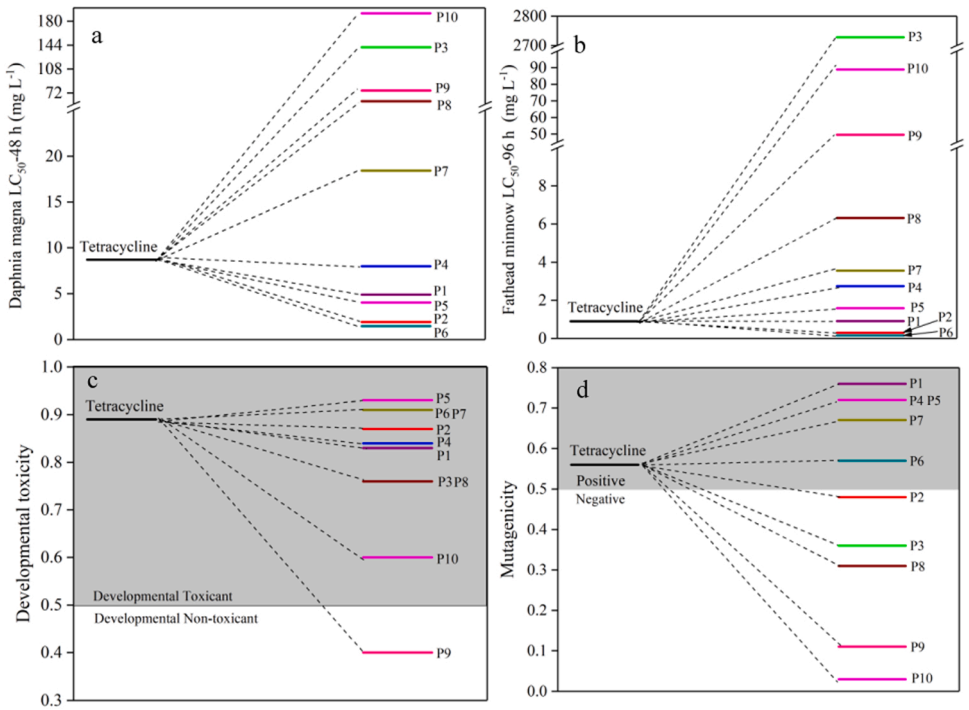

Fig. 10. The Daphnia magna LC_{50}-48 h (a), fathead minnow LC_{50}-96 h (b), developmental toxicity (c) and mutagenicity (d) of tetracycline and its possible degradation intermediates.

Similarly, Fig. 10b showed that the lethal concentration of 50% fathead minnow (LC_{50}-48 h) value of most intermediates, except for P2 (0.29 mg L^{-1}) and P6 (0.15 mg L^{-1}), were obviously higher than tetracycline (0.9 mg L^{-1}). Although relatively high acute toxicity for fathead minnow of P2 and P6 was observed, whereas the LC_{50}-96 h of their further intermediates was lower than that of tetracycline. The above results indicated that the acute toxicity of tetracycline to Daphnia magna and fathead minnow might be reduced after hetero-PEF degradation by $CuFeO_2$-NO/PBC-GDE-1.0 cathode. Furthermore, Fig. 10c and d illustrated that the developmental toxicity and mutagenicity of tetracycline exceeded 0.5, suggesting that tetracycline was "developmental toxicant" and "mutagenicity positive". As shown in Fig. 10c, the developmental toxicity of intermediates, except for P5 (0.93), P6 (0.91) and P7 (0.91), was lower than that of tetracycline (0.89), and the P9 (0.4) even changed to "developmental non-toxicant". The P5, P6 and P7 possessed high toxicity, whereas their subsequent degradation products P8 (0.76), P9 (0.4) and P10 (0.6) existed lower developmental toxicity than that of tetracycline. For the mutagenicity (Fig. 10d), the mutagenicity (<0.5) of intermediates P2, P3, P8, P9 and P10 became from "positive" into "negative". According to the above toxicity analysis, the comprehensive toxicity of tetracycline could be relieved after 180 min in hetero-PEF system.

Additionally, the removal efficiency of TOC was investigated within 420 min, and the *Escherichia coli* growth inhibition experiment was performed to assess the antibacterial property of tetracycline and reaction samples (Fig. 11 and Fig. 12). The TOC removal rate was only 33.6% in hetero-PEF system after 180 min (Fig. 11a), which was significantly lower than the degradation efficiency (96.1%) of tetracycline in the same reaction time (Fig. 4a). The present result further revealed the incomplete mineralization of tetracycline and the production of intermediates in hetero-PEF system within 180 min degradation. The *Escherichia coli* growth inhibition rate decreased from the 92.8% of tetracycline solution to 55.4% of reaction samples after 180 min degradation (Fig. 11b). Meanwhile, the *Escherichia coli* inhibition zone diameter decreased from the 12.0 mm of tetracycline solution (Figs. 12a) to 9.7 mm of reaction samples after 180 min degradation (Fig. 12b). The experimental results of *Escherichia coli* growth inhibition indicated that antimicrobial activity of intermediates produced after

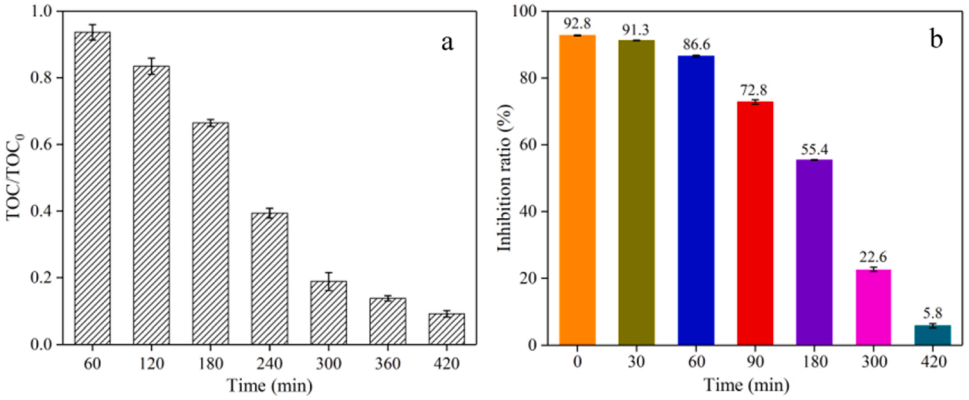

Fig. 11. TOC removal in various reaction times (a), *Escherichia coli* growth inhibition ratio of tetracycline solution and reaction samples (b).

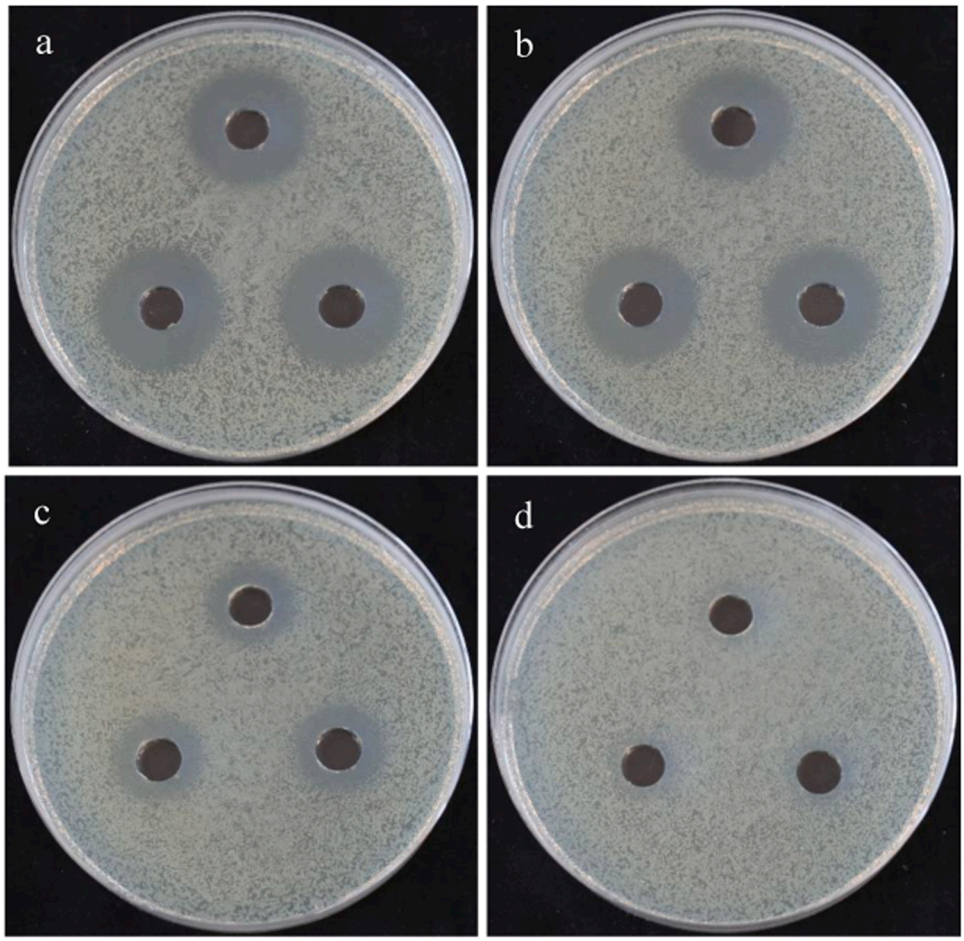

Fig. 12. *Escherichia coli* inhibition zone of initial tetracycline solution (a), the samples after 180 min (b), 300 min (c) and 420 min (d) degradation.

180 min reaction had a certain declined in hetero-PEF system. The TOC removal rate and *Escherichia coli* growth inhibition rate were 92.8% and 5.8% within 420 min, respectively (Fig. 11). Likewise, *Escherichia coli* inhibition zone diameter was also further reduced to 2.0 mm after 300 min (Fig. 12c) and had almost disappeared after 420 min (Fig. 12d). Based on the above result, hetero-PEF system with $CuFeO_2$-NO/PBC-GDE-1.0 as cathode may be a promising technique for alleviating the harms of tetracycline to environment.

4. Conclusions

The NO/PBC and $CuFeO_2$-NO/PBC were prepared by pyrolysis method and hydrothermal method, respectively. The composite GDEs with the mixture of $CuFeO_2$-NO/PBC and NO/PBC as cathode catalyst were fabricated and employed as cathode for the hetero-PEF degradation of tetracycline. The fabricated GDEs could not only produce H_2O_2 through 2-electron ORR, but also activate H_2O_2 by $CuFeO_2$ to produce active radicals. The $CuFeO_2$-NO/PBC-GDE-1.0 with the $CuFeO_2$-NO/PBC to NO/PBC ratio of 1:1 mixture as cathode catalyst has the best performance for tetracycline degradation in hetero-PEF system among as-fabricated composite GDEs, which acquired 96.1% tetracycline (20 mg L^{-1}) degradation efficiency after 180 min under 80 mA cm^{-2} and pH 5.0. Cl^- and NO_3^- had no inhibitory effect on tetracycline degradation, while HCO_3^- and HPO_4^{2-} inhibited tetracycline degradation. The recycling degradation experiments demonstrated the stability of hetero-PEF system under long-term operation. The active species quenching experiment and ESR analysis indicated that $^{\bullet}OH$ and $^{\bullet}O_2^-$ played the primary and auxiliary roles for tetracycline degradation, respectively. The electron on the cathode surface and photoinduced electron could react with $\equiv Fe^{3+}$ and $\equiv Cu^{2+}$ to generate $\equiv Fe^{2+}$ and $\equiv Cu^{+}$, promoting active radical production and tetracycline degradation. The toxicity prediction of tetracycline and its intermediates confirmed that the acute toxicity, developmental toxicity and mutagenicity of tetracycline was relieved by hetero-PEF degradation. The results of TOC removal determination and the *Escherichia coli* growth inhibition experiments within 420 min indicated that hetero-PEF system could achieve mineralization and inhibit antibacterial property of tetracycline.

CRediT authorship contribution statement

Shuaishuai Xin: Investigation, Formal analysis, Writing – original draft. **Siyue Huo:** Investigation, Formal analysis. **Yanjun Xin:** Supervision, Funding acquisition. **Mengchun Gao:** Conceptualization, Writing – review & editing, Supervision, Funding acquisition. **Yanhao Wang:** Investigation. **Wenjie Liu:** Investigation. **Chunlei Zhang:** Investigation. **Xiaoming Ma:** Investigation.

Declaration of Competing Interest

The authors declare that they have no known competing financial interests or personal relationships that could have appeared to influence the work reported in this paper.

Acknowledgements

This work is financially supported by National Natural Science Foundation of China (No. 52070107) and Fundamental Research Funds

for the Central Universities (No. 201964003).

Appendix A. Supporting information

Supplementary data associated with this article can be found in the online version at doi:10.1016/j.apcatb.2022.121442.

References

[1] T. Luo, H. Feng, L. Tang, Y. Lu, W. Tang, S. Chen, J. Yu, Q. Xie, X. Ouyang, Z. Chen, Efficient degradation of tetracycline by heterogeneous electro-Fenton process using Cu-doped Fe@Fe_2O_3: mechanism and degradation pathway, Chem. Eng. J. 382 (2020), 122970, https://doi.org/10.1016/j.cej.2019.122970.

[2] L. Xu, W. Ouyang, Y. Qian, C. Su, J. Su, H. Chen, High-throughput profiling of antibiotic resistance genes in drinking water treatment plants and distribution systems, Environ. Pollut. 213 (2016) 119–126, https://doi.org/10.1016/j.envpol.2016.02.013.

[3] Z. Zhang, Y. Chen, P. Wang, Z. Wang, C. Zuo, W. Chen, T. Ao, Facile fabrication of N-doped hierarchical porous carbons derived from soft-templated ZIF-8 for enhanced adsorptive removal of tetracycline hydrochloride from water, J. Hazard. Mater. 423 (2022), 127103, https://doi.org/10.1016/j.jhazmat.2021.127103.

[4] M. Liu, Z. Zhao, W. Yu, Comparative investigation on removal characteristics of tetracycline from water by modified wood membranes with different channel walls, Sci. Total Environ. 775 (2021), 145617, https://doi.org/10.1016/j.scitotenv.2021.145617.

[5] S. Shao, Y. Hu, J. Cheng, Y. Chen, Effects of carbon source, nitrogen source, and natural algal powder-derived carbon source on biodegradation of tetracycline (TEC), Bioresour. Technol. 288 (2019), 121567, https://doi.org/10.1016/j.biortech.2019.121567.

[6] S. Xin, G. Liu, X. Ma, J. Gong, B. Ma, Q. Yan, Q. Chen, D. Ma, G. Zhang, M. Gao, Y. Xin, High efficiency heterogeneous Fenton-like catalyst biochar modified $CuFeO_2$ for the degradation of tetracycline: economical synthesis, catalytic performance and mechanism, Appl. Catal. B Environ. 280 (2021), 119386, https://doi.org/10.1016/j.apcatb.2020.119386.

[7] G. Yang, Y. Liang, Z. Xiong, J. Yang, K. Wang, Z. Zeng, Molten salt-assisted synthesis of Ce_4O_7/Bi_4MoO_9 heterojunction photocatalysts for photo-Fenton degradation of tetracycline: enhanced mechanism, degradation pathway and products toxicity assessment, Chem. Eng. J. 425 (2021), 130689, https://doi.org/10.1016/j.cej.2021.130689.

[8] J. Zhang, S. Qiu, H. Feng, T. Hu, Y. Wu, T. Luo, W. Tang, D. Wang, Efficient degradation of tetracycline using core–shell Fe@Fe_2O_3-CeO_2 composite as novel heterogeneous electro-Fenton catalyst, Chem. Eng. J. 428 (2022), 131403, https://doi.org/10.1016/j.cej.2021.131403.

[9] Y. Wang, H. Zhang, J. Zhang, C. Lu, Q. Huang, J. Wu, F. Liu, Degradation of tetracycline in aqueous media by ozonation in an internal loop-lift reactor, J. Hazard. Mater. 192 (2011) 35–43, https://doi.org/10.1016/j.jhazmat.2011.04.086.

[10] J. Liu, H. Lin, Y. Dong, Y. He, C. Liu, MoS_2 nanosheets loaded on collapsed structure zeolite as a hydrophilic and efficient photocatalyst for tetracycline degradation and synergistic mechanism, Chemosphere 287 (2022), 132211, https://doi.org/10.1016/j.chemosphere.2021.132211.

[11] Y. Xia, F. Yang, B. Zhang, C. Xu, W. Yang, Y. Li, Fabrication of novel FeS_2 NWs/Ti_3C_2 cathode for photo-Electro-Fenton degradation of sulfamethazine, Chem. Eng. J. 426 (2021), 130719, https://doi.org/10.1016/j.cej.2021.130719.

[12] P. Su, M. Zhou, X. Lu, W. Yang, G. Ren, J. Cai, Electrochemical catalytic mechanism of N-doped graphene for enhanced H_2O_2 yield and in-situ degradation of organic pollutant, Appl. Catal. B Environ. 245 (2019) 583–595, https://doi.org/10.1016/j.apcatb.2018.12.075.

[13] J. Hu, J. Sun, J. Yan, K. Lv, C. Zhong, K. Deng, J. Li, A novel efficient electrode material: activated carbon fibers grafted by ordered mesoporous carbon, Electrochem. Commun. 28 (2013) 67–70, https://doi.org/10.1016/j.elecom.2012.11.034.

[14] J. Hu, S. Wang, J. Yu, W. Nie, J. Sun, S. Wang, Duet Fe_3C and FeNx sites for H_2O_2 generation and activation toward enhanced electro-Fenton performance in wastewater treatment, Environ. Sci. Technol. 55 (2021) 1260–1269, https://doi.org/10.1021/acs.est.0c06825.

[15] Q. Zhang, M. Zhou, G. Ren, Y. Li, X. Du, Highly efficient electrosynthesis of hydrogen peroxide on a superhydrophobic three-phase interface by natural air diffusion, Nat. Commun. 11 (2020) 1731, https://doi.org/10.1038/s41467-020-15597-y.

[16] J. Liu, X.J. Sun, P. Song, Y.W. Zhang, W. Xing, W.L. Xu, High-performance oxygen reduction electrocatalysts based on cheap carbon black, nitrogen, and trace iron, Adv. Mater. 25 (2013) 6879–6883, https://doi.org/10.1002/adma.201302786.

[17] Y. Sheng, Y. Zhao, X. Wang, R. Wang, T. Tang, Electrogeneration of H_2O_2 on a composite acetylene black–PTFE cathode consisting of a sheet active core and a dampproof coating, Electrochim. Acta 133 (2014) 414–421, https://doi.org/10.1016/j.electacta.2014.04.071.

[18] W. Zhou, L. Rajic, L. Chen, K. Kou, Y. Ding, X. Meng, Y. Wang, B. Mulaw, J. Gao, Y. Qin, A.N. Alshawabkeh, Activated carbon as effective cathode material in iron-free electro-Fenton process: Integrated H_2O_2 electrogeneration, activation, and pollutants adsorption, Electrochim. Acta 296 (2019) 317–326, https://doi.org/10.1016/j.electacta.2018.11.052.

[19] H. He, B. Jiang, J. Yuan, Y. Liu, X. Bi, S. Xin, Cost-effective electrogeneration of H_2O_2 utilizing HNO_3 modified graphite/polytetrafluoroethylene cathode with exterior hydrophobic film, J. Colloid Interface Sci. 533 (2019) 471–480, https://doi.org/10.1016/j.jcis.2018.08.092.

[20] Y. Yang, F. He, Y. Shen, X. Chen, H. Mei, S. Liu, Y. Zhang, A biomass derived N/C-catalyst for the electrochemical production of hydrogen peroxide, Chem. Commun. 53 (2017) 9994–9997, https://doi.org/10.1039/C7CC04819J.

[21] Y.H. Lee, L. Feng, K.H. Chang, C.C. Hu, T. Ohsaka, Novel synthesis of N-doped porous carbons from collagen for electrocatalytic production of H_2O_2, Appl. Catal. B Environ.. 126 (2012) 208–214, https://doi.org/10.1016/j.apcatb.2012.06.031.

[22] G. Daniel, Y. Zhang, S. Lanzalaco, F. Brombin, C. Durante, Chitosan-derived nitrogen-doped carbon electrocatalyst for a sustainable upgrade of oxygen reduction to hydrogen peroxide in UV-assisted electro-Fenton water treatment, ACS Sustain. Chem. Eng.. 38 (2020) 14425–14440, https://doi.org/10.1021/acssuschemeng.0c04294.

[23] Z. Lu, G. Chen, S. Siahrostami, Z. Chen, Yi Cui, High-efficiency oxygen reduction to hydrogen peroxide catalysed by oxidized carbon materials, Nat. Catal. 1 (2018) 156–162, https://doi.org/10.1038/s41929-017-0017-x.

[24] T.P. Fellinger, F. Hasché, P. Strasser, M. Antonietti, Mesoporous nitrogen-doped carbon for the electrocatalytic synthesis of hydrogen peroxide, J. Am. Chem. Soc. 134 (2012) 4072–4075, https://doi.org/10.1021/ja300038p.

[25] M. Qin, S. Fan, L. Wang, G. Gan, X. Wang, J. Cheng, Z. Hao, X. Li, Oxygen and nitrogen co-doped ordered mesoporous carbon materials enhanced the electrochemical selectivity of O_2 reduction to H_2O_2, J. Colloid Interface Sci. 562 (2020) 540–549, https://doi.org/10.1016/j.jcis.2019.11.080.

[26] C. Zhao, S. Zhang, M. Han, X. Zhang, Y. Liu, W. Li, C. Chen, G. Wang, H. Zhang, H. Zhao, Ambient electrosynthesis of ammonia on a biomass-derived nitrogen-doped porous carbon electrocatalyst: Contribution of pyridinic nitrogen, ACS Energy Lett. 4 (2019) 377–383, https://doi.org/10.1021/acsenergylett.8b02138.

[27] S. Meng, Z. Mo, Z. Li, R. Guo, N. Liu, Oxygen-rich porous carbons derived from alfalfa flowers for high performance supercapacitors, Mater. Chem. Phys. 246 (2020), 122830, https://doi.org/10.1016/j.matchemphys.2020.122830.

[28] Y.K. Choi, E. Kan, Effects of pyrolysis temperature on the physicochemical properties of alfalfa-derived biochar for the adsorption of bisphenol A and sulfamethoxazole in water, Chemosphere 218 (2019) 741–748, https://doi.org/10.1016/j.chemosphere.2018.11.151.

[29] S.S. Xin, Y.F. Li, J. Guan, B.R. Ma, C.L. Zhang, X.M. Ma, W.J. Liu, Y.J. Xin, M. C. Gao, Electrocatalytic oxygen reduction to hydrogen peroxide through a biomass-derived nitrogen and oxygen self-doped porous carbon metal-free catalyst, J. Mater. Chem. A 9 (2021) 25136–25149, https://doi.org/10.1039/d1ta06955a.

[30] C.M. Sánchez-Sánchez, E. Expósito, J. Casado, V. Montiel, Goethite as a more effective iron dosage source for mineralization of organic pollutants by electro-Fenton process, Electrochem. Commun. 9 (2007) 19–24, https://doi.org/10.1016/j.elecom.2006.08.023.

[31] Z. Ye, J.A. Padilla, E. Xuriguera, J.L. Beltran, F. Alcaide, E. Brillas, I. Sirés, A highly stable metal–organic framework-engineered FeS_2/C nanocatalyst for heterogeneous electro-Fenton treatment: validation in wastewater at mild pH, Environ. Sci. Technol. 54 (2020) 4664–4674, https://doi.org/10.1021/acs.est.9b07604.

[32] S. Amali, M. Zarei, M. Ebratkhahan, A. Khataee, Preparation of Fe@Fe_2O_3/3D graphene composite cathode for electrochemical removal of sulfasalazine, Chemosphere 273 (2021), 128581, https://doi.org/10.1016/j.chemosphere.2020.128581.

[33] C. Zhang, F. Li, R. Wen, H. Zhang, P. Elumalai, Q. Zheng, H. Chen, Y. Yang, M. Huang, G. Ying, Heterogeneous electro–Fenton using three-dimension NZVI–BC electrodes for degradation of neonicotinoid wastewater, Water Res. 182 (2020), 115975, https://doi.org/10.1016/j.watres.2020.115975.

[34] T. Hu, F. Deng, H. Feng, J. Zhang, B. Shao, C. Feng, W. Tang, L. Tang, Fe/Co bimetallic nanoparticles embedded in MOF-derived nitrogen-doped porous carbon rods as efficient heterogeneous electro-Fenton catalysts for degradation of organic pollutants, Appl. Mater. Today 24 (2021), 101161, https://doi.org/10.1016/j.apmt.2021.101161.

[35] Y. Wang, M. Zhao, C. Hou, W. Chen, S. Li, R. Ren, Z. Li, Efficient degradation of perfluorooctanoic acid by solar photo-electro-Fenton like system fabricated by MOFs/carbon nanofibers composite membrane, Chem. Eng. J. 414 (2021), 128940, https://doi.org/10.1016/j.cej.2021.128940.

[36] L. Cui, Q. Li, B. Chen, J. Qiu, W. Jing, X. Gu, Metal-semiconductor electron-rich interface governs the enhanced activity of spinel ferrite toward heterogeneous electro-Fenton process, Appl. Surf. Sci. 567 (2021), 150874, https://doi.org/10.1016/j.apsusc.2021.150874.

[37] N. Schmachtenberg, S. Silvestri, J. da Silveira Salla, G.L. Dotto, D. Hotza, S.L. Jahn, E.L. Foletto, Preparation of delafossite-type $CuFeO_2$ powders by conventional and microwave–assisted hydrothermal routes for use as photo-Fenton catalysts, J. Environ. Chem. Eng. 7 (2019), 102954, https://doi.org/10.1016/j.jece.2019.102954.

[38] Chu Dai, Xike Tian, Yulun Nie, Hong-Ming Lin, Chao Yang, Surface facet of $CuFeO_2$ nanocatalyst: a key parameter for H_2O_2 activation in Fenton-like reaction and organic pollutant degradation, Environ. Sci. Technol. 52 (2018) 6518–6525, https://doi.org/10.1021/acs.est.8b01448.

[39] F. Darkhosh, M. Lashanizadegan, A.R. Mahjoub, A.H. Cheshme Khavar, One pot synthesis of $CuFeO_2$@expanding perlite as a novel efficient floating catalyst for rapid degradation of methylene blue under visible light illumination, Solid State Sci. 91 (2019) 61–72, https://doi.org/10.1016/j.solidstatesciences.2019.03.009.

[40] S. Xin, B. Ma, G. Liu, X. Ma, C. Zhang, X. Ma, M. Gao, Y. Xin, Enhanced heterogeneous photo-Fenton-like degradation of tetracycline over $CuFeO_2$/biochar

catalyst through accelerating electron transfer under visible light, J. Environ. Manag. 285 (2021), 112093, https://doi.org/10.1016/j.jenvman.2021.112093.
[41] S. Xin, S. Huo, C. Zhang, X. Ma, W. Liu, Y. Xin, M. Gao, Coupling nitrogen/oxygen self-doped biomass porous carbon cathode catalyst with $CuFeO_2$/biochar particle catalyst for the heterogeneous visible-light driven photo-electro-Fenton degradation of tetracycline, Appl. Catal. B Environ. 305 (2022), 121024, https://doi.org/10.1016/j.apcatb.2021.121024.
[42] T.P. Fellinger, F. Hasché, P. Strasser, M. Antonietti, Mesoporous nitrogen-doped carbon for the electrocatalytic synthesis of hydrogen peroxide, J. Am. Chem. Soc. 134 (2012) 4072–4075, https://doi.org/10.1021/ja300038p.
[43] L. Li, C. Tang, Y. Zheng, B. Xia, S. Qiao, Tailoring selectivity of electrochemical hydrogen peroxide generation by tunable pyrrolic-nitrogen-carbon, Adv. Energy Mater. 10 (2020), 2000789, https://doi.org/10.1002/aenm.202000789.
[44] J. Zhang, G. Zhang, S. Jin, Y. Zhou, J. Qu, Graphitic N in nitrogen-doped carbon promotes hydrogen peroxide synthesis from electrocatalytic oxygen reduction, Carbon 163 (2020) 154–161, https://doi.org/10.1016/j.carbon.2020.02.084.
[45] H.L. Wang, T.H. Chen, D. Chen, X. Zou, M. Li, F. Huang, F. Sun, C. Wang, D. Shu, H. Liu, Sulfurized oolitic hematite as a heterogeneous Fenton-like catalyst for tetracycline antibiotic degradation, Appl. Catal. B Environ. 260 (2020), 118203, https://doi.org/10.1016/j.apcatb.2019.118203.
[46] Y. Liu, X. He, Y. Fu, D.D. Dionysiou, Degradation kinetics and mechanism of oxytetracycline by hydroxyl radical-based advanced oxidation processes, Chem. Eng. J. 284 (2016) 1317–1327, https://doi.org/10.1016/j.cej.2015.09.034.
[47] G. Mark, H.G. Korth, H.P. Schuchmann, C. von Sonntag, The photochemistry of aqueous nitrate ion revisited, J. Photochem. Photobiol. A Chem. 101 (1996) 89–103, https://doi.org/10.1016/S1010-6030(96)04391-2.
[48] P. Neta, R.E. Huie, Rate constants for reactions of nitrogen oxide (NO_3) radicals in aqueous solutions, J. Phys. Chem. B 90 (1986) 4644–4648, https://doi.org/10.1021/j100410a035.
[49] Y. Ding, H. Tang, S. Zhang, S. Wang, H. Tang, Efficient degradation of carbamazepine by easily recyclable microscaled $CuFeO_2$ mediated heterogeneous activation of peroxymonosulfate, J. Hazard. Mater. 317 (2016) 686–694, https://doi.org/10.1016/j.jhazmat.2016.06.004.
[50] Y. Ding, W. Huang, Z. Ding, G. Nie, H. Tang, Dramatically enhanced Fenton oxidation of carbamazepine with easily recyclable microscaled CuFeO2 by hydroxylamine: kinetic and mechanism study, Sep. Purif. Technol. 168 (2016) 223–231, https://doi.org/10.1016/j.seppur.2016.05.043.
[51] J. Jiang, X. Wang, Y. Liu, Y. Ma, T. Li, Y. Lin, T. Xie, S. Dong, Photo-Fenton degradation of emerging pollutants over Fe-POM nanoparticle/porous and ultrathin g-C_3N_4 nanosheet with rich nitrogen defect: degradation mechanism, pathways, and products toxicity assessment, Appl. Catal. B Environ. 278 (2020), 119349, https://doi.org/10.1016/j.apcatb.2020.119349.
[52] B. Gao, S. Dong, J. Liu, L. Liu, Q. Feng, N. Tan, T. Liu, L. Bo, L. Wang, Identification of intermediates and transformation pathways derived from photocatalytic degradation of five antibiotics on $ZnIn_2S_4$, Chem. Eng. J. 304 (2016) 826–840, https://doi.org/10.1016/j.cej.2016.07.029.